



Influence of temperature on the process of hydrogen bond symmetrization in ϵ -FeOOHZhen-Shuai Lei ^{1,2}, Xiao-Wei Sun,^{1,*} Xin-Xuan Wang,¹ Zi-Jiang Liu,¹ Ting Song,¹ and Jun-Hong Tian¹¹*School of Mathematics and Physics, Lanzhou Jiaotong University, Lanzhou 730070, China*²*Faculty of Science, Wuhan University of Technology, Wuhan 430079, China* (Received 25 May 2023; revised 24 August 2023; accepted 2 November 2023; published 17 November 2023)

Investigating hydrogen bond symmetrization in hydroxyl compounds necessitates the precise determination of crystal microstructures. Nonetheless, H atoms are nearly indistinguishable in experiments, posing a challenge to unraveling the formation mechanism of this phenomenon. A deep learning potential model was used for classical molecular dynamics simulations of the hydrogen bond symmetrization process of ϵ -FeOOH in this study. Through calculations of the H–O bond length, it has been determined that the system undergoes hydrogen bond symmetrization when the pressure reaches 40.25 GPa. The volume thermal expansion curve of ϵ -FeOOH exhibits anomalies due to the proton-disordering phase transition, and the pressure for this transition shows a negative correlation with temperature. The calculated results of the $O_1 \cdots O_2$ bond length indicate that an increase in temperature will lead to an increase in the critical pressure for hydrogen bond symmetrization while reducing the distinction between the hydrogen bond symmetrization structure and the proton-disordered structure. In addition, the spin transition of Fe atoms at lower temperatures is unrelated to hydrogen bond symmetrization. However, with increasing temperature, the spin transition may potentially promote hydrogen bond symmetrization.

DOI: [10.1103/PhysRevB.108.184105](https://doi.org/10.1103/PhysRevB.108.184105)**I. INTRODUCTION**

FeOOH, an abundant water-bearing mineral found in the Earth's crust and mantle, exerts significant influence over terrestrial life and crucial physical and chemical processes within the planet's interior [1]. Recent studies reveal the capacity of FeOOH to transport water deeply into the Earth's interior via subducting slabs [2,3], accompanied by a complex series of structural phase transitions. Under ambient pressure, FeOOH is stable as the goethite phase (α -FeOOH) [4,5]; both akaganeite (β -FeOOH) and lepidocrocite (γ -FeOOH) are metastable phases [6,7]. In the pressure range of 5–8 GPa, α -FeOOH transforms to the high-pressure phase (ϵ -FeOOH) [7–9], which progressively undergoes second-order and first-order phase transitions of $P2_1nm \rightarrow Pnmm \rightarrow Pnmm$ due to hydrogen bond symmetrization and spin transition [7,10–12]. At a pressure of 90 GPa at 1500 K, pyrite-type FeOOH appears and stabilizes to 129 GPa [13,14], which also predicts that FeOOH is expected to be the main mineral to undertake the Earth's water cycle task.

The hydrogen bond symmetrization refers to the gradual transformation of the asymmetric $O_1\text{—}H \cdots O_2$ bond in ϵ -FeOOH into a symmetrical bond, thereby triggering a second-order phase transition from $P2_1nm$ structure to a higher-symmetry structure with the $Pnmm$ space group. During this process, the volume change is continuous. This phenomenon is also observed in other materials, including ice, AlOOH(D), CrOOH(D), GaOOH, InOOH, and more [15–18]. Accurately determining the pressure of hydrogen bond

symmetrization in ϵ -FeOOH is of utmost significance. Prior studies suggested that this phenomenon may have a connection with H/D chemical differentiation in the deep Earth induced by H isotope effects [15] and may also act as an ancillary factor in the spin transition of ϵ -FeOOH [11]. Even more interesting, the increased strength of the bonds due to the increased symmetry of the hydrogen bonds is likely to help enhance the stability of hydrous minerals in the Earth's interior, which is critical to understanding how water is stored and recycled deep within the Earth's interior [19]. That is, by employing ϵ -FeOOH as a representative mineral, we can establish a universal principle of hydrogen bond symmetrization applicable to all compounds of similar nature. However, a considerable discrepancy exists in the literature regarding the hydrogen bond symmetrization pressure of FeOOH. Specifically, Gleason *et al.* [11] used the first-principles calculations to determine the hydrogen bond symmetrization pressure to be 43 GPa and postulated that the hydrogen bond symmetrization triggers a spin transition. The experimental results obtained by Xu *et al.* [20] exceeded 44 GPa and presented the opposite conclusion to Gleason *et al.* [11] that the spin transition caused the hydrogen bond symmetrization. The experimental results of Thompson *et al.* [21] showed that the ϵ -FeOOH undergoes the hydrogen bond symmetrization (or disorder) at 18 GPa, which is much lower than other results available, so they suggested that the hydrogen bond symmetrization is unlikely to be related to the high-low spin transition. The reason for such a significant difference in the hydrogen bond symmetrization pressure of ϵ -FeOOH may be influenced by the proton-disordering phase transition. We speculate that the room-temperature x-ray-diffraction experiments by Thompson *et al.* [21] probably detected the proton-disordered phase

*sunxw_lzjtu@yeah.net

of ε -FeOOH. Proton disorder is a precursor to hydrogen bond symmetrization, and only the vibrational behavior of the H atoms in these two structures differs slightly, resulting in diffraction patterns that are almost indistinguishable [22]. Additionally, x-ray diffraction makes the identification of H atoms difficult due to its inherent dependence on electron density, which greatly increases the possibility of this speculation. In general, the experimental challenges and the absence of theoretical research addressing the impact of temperature on the dynamics of the local structure of ε -FeOOH constrain our in-depth comprehension of the hydrogen bond symmetrization phenomenon.

A recent report by Meier *et al.* [23] showed that the hydrogen bond symmetrization in different systems all occurs at the critical point where the H atom flows fastest and is independent of the chemical environment of the H atom, a conclusion they reached from their recent high-pressure nuclear magnetic resonance spectroscopy experiments, which is probably the most revealing study to date on the nature of the hydrogen bond symmetrization. This conclusion also implied that temperature may play an important role in the second-order phase transition of ε -FeOOH because of its ability to increase the vibrational frequency of the H atoms. Therefore, the present study aims to investigate the effect of temperature on the structure of $O_1-H \cdots O_2$ bonds under high pressure and to resolve the pressure differences of the hydrogen bond symmetrization phenomenon. However, it is challenging to experimentally detect H atoms, and even the latest experimental tools are difficult to obtain the hydrogen bond dynamics behavior of the whole hydrogen bond symmetrization process, while density-functional theory (DFT) simulations with statistical properties for many atoms are also difficult, and the above facts lead to an obstacle to the implementation of this study. The classical molecular dynamics (MD) simulations methods may be an effective way to solve the above dilemma. Aryanpour *et al.* [24] proposed a reactive force field that can be used for α -FeOOH, and this force field gave good results in the water- α -FeOOH system, but no potential function applicable to ε -FeOOH was seen. Therefore, if our conjecture is to be verified by MD simulations, the support of a reliable potential function model is needed first. Recently, several approaches based on machine learning for force-field fitting have gradually come into the limelight, such as deep potential molecular dynamics (DPMD) [25,26], Behler-Parrinello neural network [27], gradient-domain machine learning [28], Gaussian approximation potentials [29], spectral neighbor analysis potential [30], and so on, where DPMD has an accuracy very close to the DFT results, allowing us to achieve FeOOH force-field fitting for high-precision large-scale molecular simulations. Here, we have computationally investigated the relationship between the hydrogen bond symmetrization phenomenon and the temperature of ε -FeOOH by developing deep learning potential (DP) models applicable to α -FeOOH and ε -FeOOH.

II. COMPUTATIONAL DETAILS

The MD method allows the calculation of thermodynamic statistical properties for systems containing many atoms, which is important for studying the hydrogen bond

symmetrization phenomenon in ε -FeOOH. This is because ε -FeOOH may have a proton-disordered precursor structure before entering the hydrogen bond symmetrization structure [31], which has a hydrogen bond of $O_1-H \cdots O_2$ or $O_1 \cdots H-O_2$ bond type, i.e., there are two equilibrium positions of H atoms on the $O_1 \cdots O_2$ bond, and when the temperature effect is introduced, H atoms vibrate substantially and randomly occupy the two equilibrium positions. At this point, a larger number of samples is required for statistical analysis to obtain a general conclusion. The MD simulations in this paper are all carried out in the Large-scale Atomic/Molecular Massively Parallel Simulator (LAMMPS) software [32], with periodic boundary conditions imposed on the simulations, a conjugate gradient algorithm for energy minimization with a time step of 1 fs, and the number of atoms is 3456 for the ε -FeOOH. The potential model is fitted using a deep learning approach, and its fitting and validation will be described subsequently.

A. Construction of training set

The geometric optimization of the crystal structure of interest is first performed by the first-principles calculations to obtain the geometric configuration of the crystal at different pressures. The DFT calculations were performed in the Vienna *Ab initio* Simulation Package (VASP) [33,34]. The generalized gradient approximation (GGA) method of the Perdew-Burke-Ernzerhof form [35,36] was chosen to describe the exchange-correlation interactions between electrons during geometric optimization. However, the standard GGA method usually fails to accurately describe the electronic structure of systems containing transition metals because the strong electronic correlations of *d* and *f* electrons are often accompanied by complex magnetic variations, which in turn lead to erroneous estimates of the structural relationships by DFT calculations. For example, Otte *et al.* [7] obtained a lower spin transition pressure (7.7 GPa) for ε -FeOOH using the GGA method, while a more reasonable result can be obtained with GGA+*U* [37]. By utilizing the Hubbard parameters $U = 5$ eV and exchange parameter $J = 1$ eV, the spin transition pressure of ε -FeOOH, as calculated by Otte *et al.* [7], can be raised to 56.5 GPa. This adjustment aligns the calculated value more closely with the experimental findings within the range of 40–60 GPa [11,20]. In the present work, U and J were also taken as 5 and 1 eV, respectively, and this set of parameters has also been successfully applied in other studies on iron oxides [38,39]. Indeed, the selection of more appropriate U and J parameters can take into account variations in crystal structure and pressure. For instance, Nishi *et al.* [14] determined the U value of ε -FeOOH in the low-spin state at different pressures based on linear response theory to accurately delineate the phase relationship between ε -FeOOH and pyrite-FeOOH. However, fitting the DP model has a high self-consistency requirement for the DFT data, which makes it necessary to choose the same U and J parameters for any condition. The good thing is that the U value does not change significantly with pressure, even within the extensive pressure range of 150 GPa; as explored in Nishi *et al.*'s study [14], the U value experiences a mere increment of 0.853 eV. The study of magnesium pyrite by Tsuchiya *et al.* [40] similarly showed

minor fluctuations in the U value, with less than 1 eV observed for a significant 30% volume change. In a study of α -Fe₂O₃, the weak effect of cell volume on the U value was emphasized by Rollmann *et al.* [39], who chose a consistent value of 4 eV to ensure overall fidelity. To determine the effect of a consistent choice of Hubbard parameters on computational results, the impact of the U value on the H–O bond length was meticulously examined (refer to Supplemental Material, Sec. S1 for further details [41]; see also Ref. [42] therein). Interestingly, each 1-eV increase in the U value was found to affect the H–O bond length equivalent to a pressure increase of 2–3 GPa. Therefore, maintaining a consistent U value may result in slightly greater H–O bond lengths under high-pressure conditions, leading to similarly slightly elevated pressure-related conclusions in this study. However, such considerations do not affect our qualitative study significantly, as the actual increase in the U value would not exceed 1 eV. For the other settings, the electron-ion interaction is described by the projector-augmented wave method [43], the plane-wave cutoff energy is set to 650 eV, the energy and force convergence criteria of the system are 1×10^{-8} eV and 0.01 eV/Å, respectively, the Brillouin-zone k points are generated by the Monkhorst-Pack method [44], and α -FeOOH and ε -FeOOH are taken to be $4 \times 11 \times 8$ and $11 \times 7 \times 7$, respectively. We also add spin polarization to the system considering the magnetic effect of Fe atoms.

The training data for the DP model have been obtained from *ab initio* molecular dynamics (AIMD) simulations with the same pseudopotential, exchange-correlation functional, GGA+ U , and magnetic settings as in the geometry optimization. Unlike the geometric optimization, we reduce the cutoff energy to 500 eV, the energy convergence criterion to 1×10^{-4} eV, and the Brillouin-zone k points are chosen as Γ points. The simulated system contains 128 atoms, which are heated from 10 to 300 K in a Nosé-Hoover thermostat [45,46] based on the *NVT* ensemble. Due to the presence of H atoms, a time step of 0.5 fs was chosen. To improve the adaptability of the DP model, the AIMD simulations were performed for α -FeOOH at pressures of 0, 5, and 10 GPa, and for ε -FeOOH at pressures of 10, 30, and 50 GPa, each with a total step number of 3000. We finally obtained the DFT dataset for training the DP model, of which 90% of the data were used as the training set and 10% as the test set. The diminished accuracy of AIMD could result in less precise calculations of H–O bond lengths, consequently perturbing the determination of hydrogen atom positions during dynamic processes. To assess the impact of the reduced computational accuracy in AIMD simulations on the simulation results, we calculated the H–O bond lengths of ε -FeOOH at various pressures with the same level of accuracy as employed in the AIMD simulations used to create the training dataset. Subsequently, we compared these results with the outcomes of geometric optimization (refer to Supplemental Material, Sec. S2 for further details [41]). The resultant analysis demonstrates that accuracy reduction induces a bond-length error ranging from 0.004 to 0.006 Å at low pressure, with this effect dwindling to 0.001–0.002 Å at 40 GPa. After the final pressure exceeds 50 GPa, the accuracy decrease no longer affects the H–O bond length. Overall, the reduction in accuracy resulted in merely a slight change in bond length, ensuring that our AIMD simulations

fulfill the requirement to accurately explore the positions of H atoms.

B. Training the potential model

The training of the DP model was performed in the DEEPMD-KIT package [25,47,48]. In the DPMD method, the total energy E is defined as the sum of the individual atomic energies E_i determined by the positions of atom i and its nearest neighbors within the cutoff radius. To keep the structure translational, rotational, and exchange symmetric in the potential-energy plane, the positions of the atoms are mapped into a descriptor that satisfies the symmetry requirement, and these descriptors are fed into the neural network for fitting the high-dimensional energy function. In this work, to achieve better linear partitioning of different types of data, three hidden layers are applied; the embedding network is 25, 50, and 100, and the fitting network is 240, 240, and 240. The cutoff radius is set to 6 Å. The initial learning rate decays exponentially every 5000 steps starting from 1×10^{-3} and decreasing to 3.51×10^{-8} at the end of the training. We set the total number of training steps to 1×10^6 for sufficient fitting accuracy and to prevent overfitting. The loss function in the training process is defined as [47]

$$L(P_\varepsilon, P_f, P_\xi) = \frac{P_\varepsilon}{N} \Delta E^2 + \frac{P_f}{3N} \sum |\Delta \mathbf{F}_i|^2 + \frac{P_\xi}{9N} \|\Delta \Xi\|^2, \quad (1)$$

where P_ε , P_f , and P_ξ are the respective weights of the learning process. We considered that the virial information, i.e., the state of the internal stresses of the system, can be derived from energy and force, so we did not include the virial data in the training and the value of P_ξ was set to 0. The initial P_ε and P_f were 0.02 and 1000, and they are made to asymptote to 1 during the training process, where ΔE , ΔF , and $\Delta \Xi$ are the root-mean square error (RMSE) of energy, force, and virial, respectively:

$$\text{RMSE} = \sqrt{\frac{1}{m} \sum_{i=1}^m (x_i - \hat{x}_i)^2}, \quad (2)$$

where m is the number of samples, x_i denotes the DFT data, and \hat{x}_i denotes the inferred data of the DP model.

C. Reliability and validation of DP

The training quality of the model is understood by comparing the DFT data with the inferred data of the DP model. It can be seen from Fig. 1 that the energy and force inferred by the DP model of FeOOH are highly consistent with the DFT results. To specify the training error, we also additionally calculated the RMSE of the model. The RMSE of energy and atom forces in x , y , and z directions are 0.14 meV/atom, 29.61 meV/Å, 29.53 meV/Å, and 30.46 meV/Å, respectively. Compared with the tests of the DPMD method in other systems [48], the potential functions obtained in this work have relatively low RMSE.

Although the DP model was verified with energy and force accuracy, we calculated the phase-transition pressure, compression curve, and thermal expansion of FeOOH to further verify the reliability of the model. The phase-transition

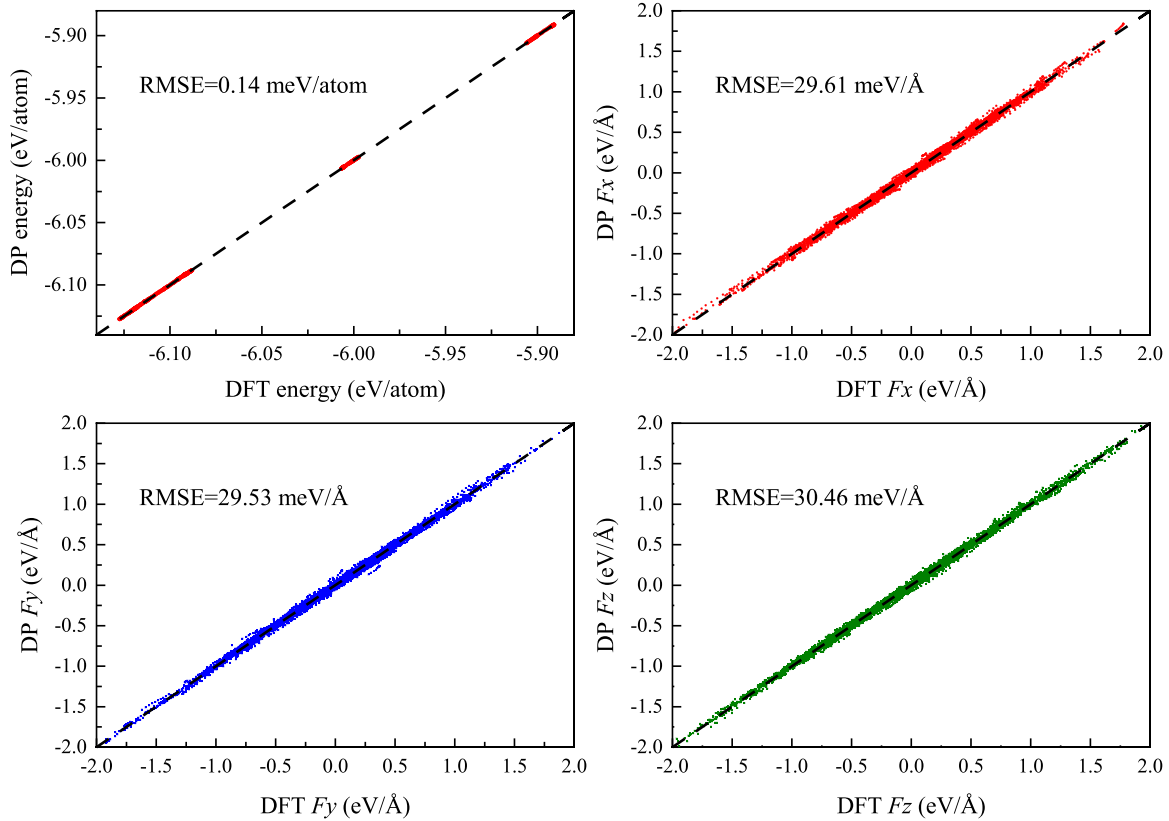
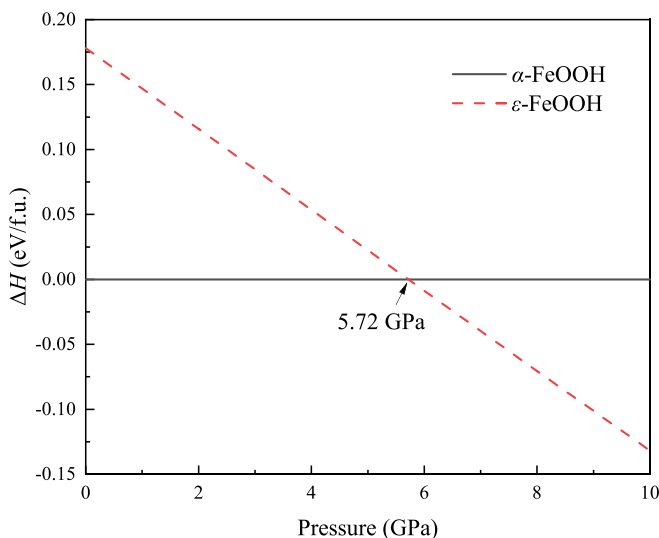


FIG. 1. Comparison of inferred results of DP model with DFT results.

pressure of the materials can be determined by finding the point where the Gibbs free energy is equal, which requires high-energy accuracy. We have calculated the phase-transition pressure of α -FeOOH and ε -FeOOH at zero temperature using the DP model. As shown in Fig. 2, the enthalpy difference between α -FeOOH and ε -FeOOH rapidly approaches with increasing pressure, and ε -FeOOH becomes the most stable phase after 5.72 GPa, which is consistent with existing results.

FIG. 2. Enthalpy difference between α -FeOOH and ε -FeOOH as function of pressure.

For example, Otte *et al.* [7], using the GGA+ U method, found that the phase transition between α -FeOOH and ε -FeOOH occurs at 5.9 GPa. The x-ray-diffraction experiments by Gleason *et al.* [49] showed that at temperatures below 200 °C and pressures above 5 GPa, α -FeOOH is metastable and gradually transforms to ε -FeOOH with increasing reaction time.

The correlation between volume and pressure plays an irreplaceable role in determining the form of minerals present in the Earth's interior. The P - V relationships for α -FeOOH and ε -FeOOH calculated using the DP model are shown in Fig. 3. For comparison, the volume of each phase is converted to the molecular formula volume. The volume of α -FeOOH at zero pressure is close to the experimental results of Nagai *et al.* [4] and then gradually approaches those of Gleason *et al.* [49], and also lies between the calculations of Otte *et al.* [7] using the GGA and GGA+ U methods. The volume of ε -FeOOH is slightly higher than the available experimental values at lower pressure [12,50,51] but approaches the experimental results of Gleason *et al.* [11] with increasing pressure.

Figure 4(a) shows the variation of the volume ratio of FeOOH with temperature for both α and ε phases. The volume of α -FeOOH increases with temperature at 0 GPa, and the bulk thermal expansion coefficient α is $2.73 \times 10^{-5} / \text{K}$ at 300 K, which is close to $2.3 (\pm 0.6) \times 10^{-5} / \text{K}$ for the x-ray-diffraction experiments [49]. For ε -FeOOH, the volume expands steadily with increasing temperature for both 0 and 50-GPa pressure conditions. However, the thermal expansion curve of ε -FeOOH at 10 GPa showed an anomaly, with its volume gradually increasing with temperature up to 300 K, while the rate of thermal expansion decreased. Then, the

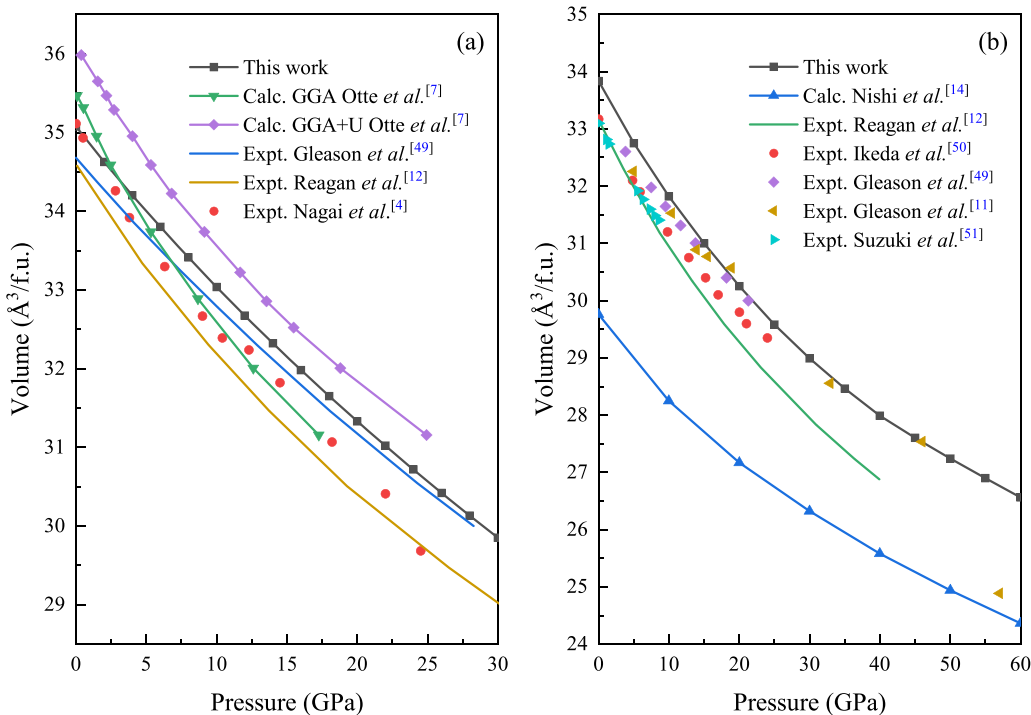


FIG. 3. Volume variation of (a) α -FeOOH and (b) ϵ -FeOOH with pressure.

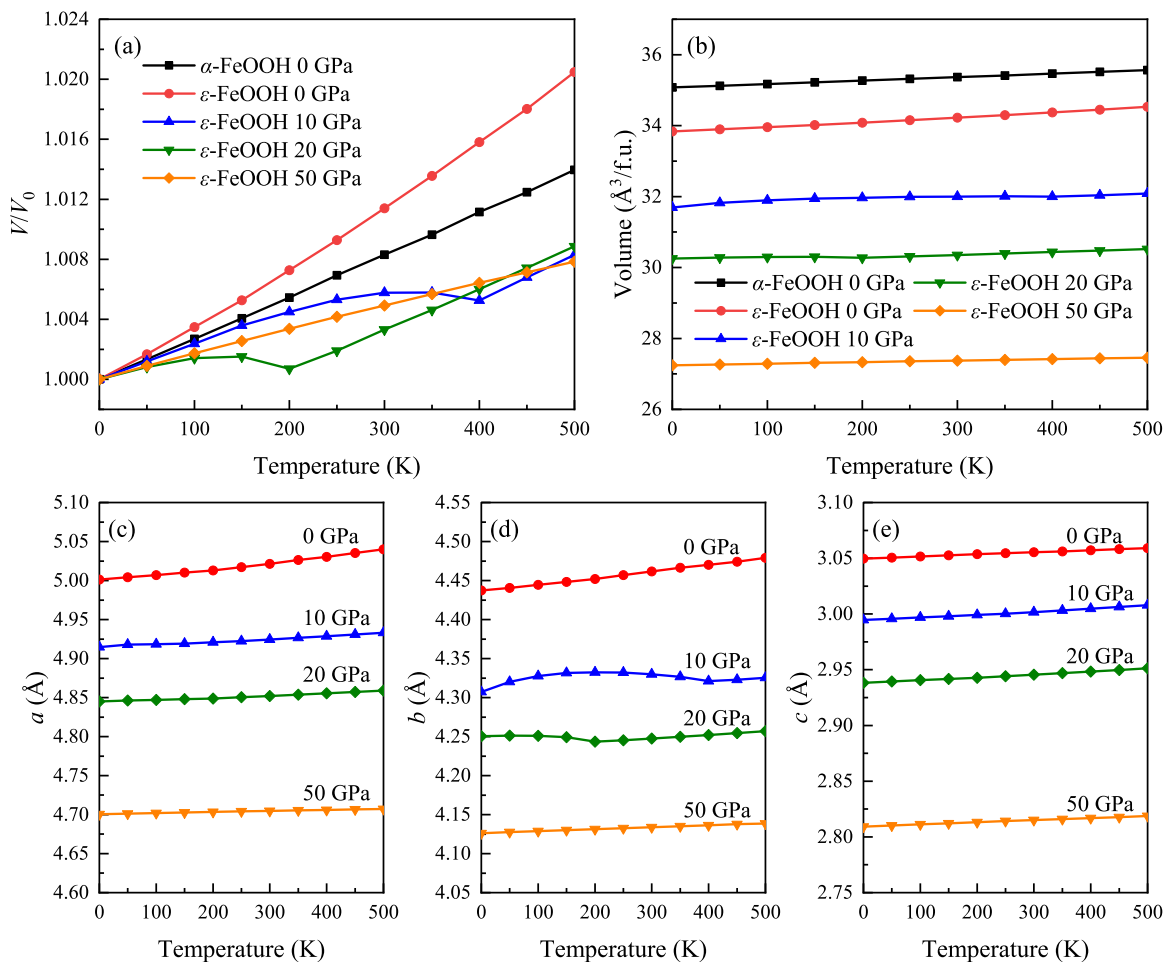


FIG. 4. Temperature dependence of structural parameters of α -FeOOH and ϵ -FeOOH in temperature range 0–500 K, where (a) is volume ratio, (b) is volume, and (c), (d), and (e) are lattice constants a , b , and c of ϵ -FeOOH, respectively.

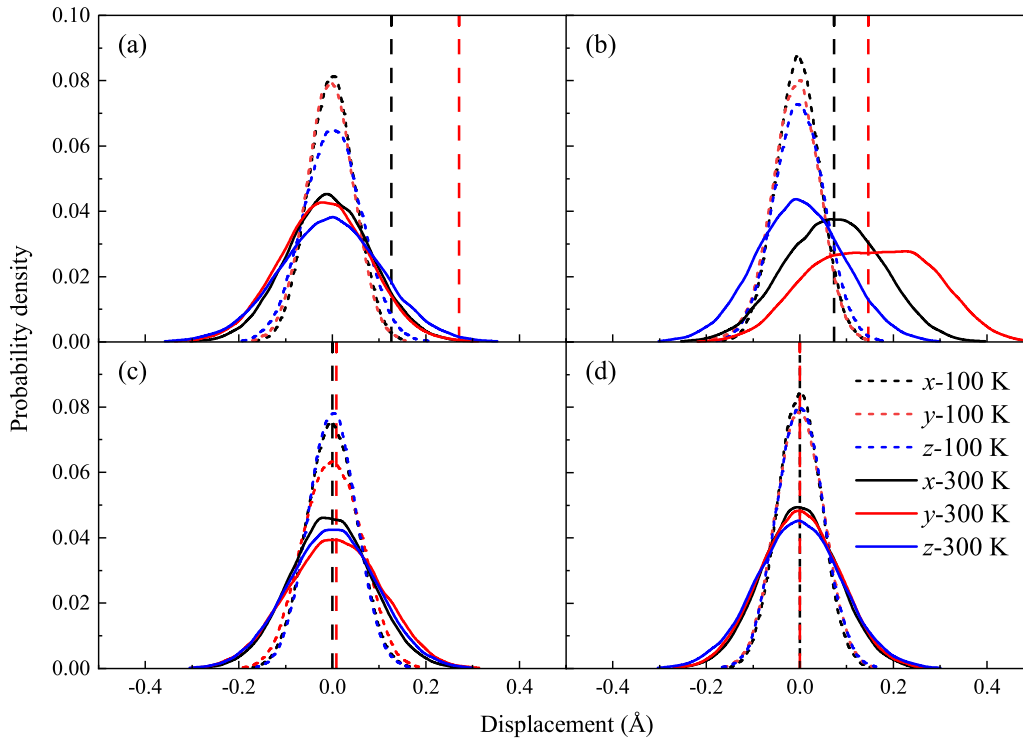


FIG. 5. H atoms displacement probability distribution function at (a) 0 GPa, (b) 20 GPa, (c) 40 GPa, and (d) 60 GPa; black and red vertical dashed lines represent (x, y) coordinates of $O_1 \cdots O_2$ centers relative to reference H atoms for respective conditions.

volume of ε -FeOOH showed a paradoxical decreasing trend between 300 and 400 K and returned to the normal thermal expansion trend after the temperature exceeded 400 K. At 20 GPa, the thermal expansion curve also shows an anomaly, but the temperature at which this anomaly occurs is reduced to 200 K. From Fig. 4(b), we can also observe a slight anomaly in the volume of ε -FeOOH at 10 and 20 GPa. Based on the lattice constants shown in Figs. 4(c) to 4(e), it is evident that this anomaly primarily occurs in the b direction of the lattice. This suggests that during the temperature increase process, ε -FeOOH likely experiences significant atomic displacements along the b axis. Furthermore, considering that the arrangement of the O_1 —H \cdots O_2 bonds has the largest component in the b axis (see Fig. 6), it is highly likely that the anomaly in the volume expansion curve results from the dynamic behavior of the H atoms in the hydrogen bonds. We will provide a more detailed analysis of this phenomenon in the next subsection.

D. Correlation between anomalous thermal expansion behavior and proton disordering

The anomalies of these thermal expansion curves in Fig. 4(a) may be linked to the dynamic behavior of the H atoms in ε -FeOOH. To corroborate this, we initially computed the probability distribution function $p(r)$ [52] for the displacements of atoms in ε -FeOOH within the pressure range of 0–60 GPa at temperatures of 100 and 300 K. The $p(r)$ for H atoms is shown in Fig. 5 (the $p(r)$ for O and Fe atoms can be found in Figs. S2 and S3 in the Supplemental Material [41]). There is no significant change in the positional distribution of H atoms when the temperature is increased from 100 to 300 K at 0 GPa. It is noteworthy that at 300 K, the $p(r)$ curves along the

x and y directions show imperfect peaks. This may be due to the asymmetric nature of hydrogen bonding. Specifically, the probability of H atoms vibrating toward two neighboring O atoms in an asymmetric position is not equal. When vibrating toward the O_1 atoms, they are subject to stronger forces and are therefore more challenging, whereas vibrating toward the O_2 atoms is relatively easier. This results in a subtle asymmetry in the position of the peaks in the $p(r)$ curve. Furthermore, the H atoms are only affected in the x (lattice a) and y (lattice b) directions. This is because the vibrational behavior of the H atom along the hydrogen bond axis in the O_1 —H \cdots O_2 bond occurs exclusively within the xy plane. Taking this into consideration, we have marked in Fig. 5 the (x, y) coordinates of the $O_1 \cdots O_2$ center relative to the reference H atom at different pressures. This helps us precisely determine the distribution of H atoms in the O_1 —H \cdots O_2 bond at various temperatures. At 20 GPa, the $p(r)$ curves of H atoms along both the x and y directions show significant rightward shifts with increasing temperature, and the peaks of the curves appear to plateau symmetrically with respect to the (x, y) coordinates of the $O_1 \cdots O_2$ centers. Moreover, the plateau in the $p(r)$ curves along the y direction is markedly broader than that along the x direction. This discrepancy implies that the vibrational range of H atoms in the y direction is more extensive compared to the x direction. This vibration behavior may be the fundamental cause of the anomalies in the b -axis lattice length and volume of ε -FeOOH, and a comprehensive analysis will follow to clarify how vibrations of H atoms affect the volume. The H atom at 40 GPa is near the midpoint of $O_1 \cdots O_2$. As the temperature increases, the probability distribution function of the H atoms exhibits a plateau shape similar to that observed at 20 GPa. It is evident

TABLE I. Crystal structures information of ϵ -FeOOH at 20 GPa pressure, at temperatures of 100 and 300 K.

Space group	100 K $P2_1nm$	300 K $Pnmm$
Lattice parameter (\AA)	$a = 4.847, b = 4.251, c = 2.941$	$a = 4.852, b = 4.247, c = 2.946$
Volume (\AA^3)	60.593	60.703
Fe	$x = 0.000, y = 0.736, z = 0.000$ $x = 0.511, y = 0.782, z = 0.000$	$x = 0.000, y = 0.000, z = 0.000$ Avg.: $x = 0.000, y = 0.500, z = 0.500^a$ R. (50%): $x = 0.017, y = 0.524, z = 0.500^a$ R. (50%): $x = -0.017, y = 0.476, z = 0.500^a$
H		
O ₁	$x = 0.645, y = 0.983, z = 0.000$	$x = 0.353, y = 0.769, z = 0.000$
O ₂	$x = 0.348, y = 0.518, z = 0.000$	

^a“Avg.” represents average position of hydrogen atom, and “R.” represents real equilibrium position of hydrogen atom.

that the width of the plateau has significantly decreased due to the pressure. At 60 GPa pressure, the positions of the H atoms no longer exhibit significant changes with increasing temperature, and their $p(r)$ curves appear highly symmetrical. The plateau characteristics that were originally present under 40 GPa pressure have also disappeared. Considering the distinctive characteristics of the $p(r)$ curves at 20 GPa under pressure, and the fact that temperatures of 100 and 300 K happen to symmetrically flank the anomalous points in the volume thermal expansion curves under this pressure, it is possible to obtain a rather stable crystal structure by tracking the atomic positions at these temperatures under this pressure condition. This enables a more in-depth analysis of the structural changes induced by temperature. The obtained atomic occupations and corresponding crystal structures are presented in Table I and Fig. 6.

The results indicate that at a pressure of 20 GPa and a temperature of 100 K, the crystal space group of ϵ -FeOOH is $P2_1nm$. The H atoms collectively approach one side of the O₁ atoms, resulting in the formation of completely asymmetric hydrogen bonds, as shown in Fig. 6(a). When the temperature reaches 300 K, the crystal structure undergoes peculiar changes. By tracking the positions of the H atoms, we discovered that their average position is precisely at the O₁ ··· O₂ centers, as indicated by the “Avg.” position in Table I. The space group determined through this position is the $Pnmm$ structure. Nevertheless, the $p(r)$ curves in Fig. 5(b) indicate that the H atoms are symmetrically distributed on both sides of the centers for the O₁ and O₂ atoms, which suggests that the H atoms do not vibrate at a fixed position, but within a certain range. Therefore, this may be a result of the H atoms jumping back and forth between the two positions. The extracted atomic position data from these trajectories also exhibit this characteristic. We extracted these two coordinates, denoted as the “R.” position in Table I, and constructed the crystal structure as shown in Fig. 6(b). These characteristics indicate that the structure corresponds to a proton-disordered state of ϵ -FeOOH, exhibiting the $Pnmm$ space group. The probability of the H atoms appearing at the two R’s is equal. This observation demonstrates that the elevation in temperature indeed prompts a phase transition in ϵ -FeOOH from a completely asymmetric hydrogen-bonded structure to a proton-disordered configuration. Based on our analysis, the fundamental reason behind the volume reduction of ϵ -FeOOH as temperature increases is that the H atoms jump, which shortens the average

distance between O₁ ··· O₂ atoms. When the H atoms in the O₁—H ··· O₂ bonds jump, the interatomic interaction forces cause slight displacements of nearby O atoms. After the H atoms reach another position, the O atoms return to their original equilibrium positions. Although the initial and final positions of the O atoms do not change during the H atoms jump, the average O₁ ··· O₂ distance is reduced. Occasional H atom jumps have a subtle impact on the average O₁ ··· O₂ distance; when the H atoms can jump at a stable frequency, the average O₁ ··· O₂ distance decreases to a local minimum. Consequently, the volume of ϵ -FeOOH decreases due to the shortened bond lengths with increasing temperature. Once the H atoms’ jump frequency surpasses this stable rate, it no longer can decrease the O₁ ··· O₂ atom distance, as a result, the volume returns to its normal trend of increasing with rising temperature. This is the underlying cause of the anomalous volume reduction in ϵ -FeOOH. Meanwhile, the fact that the lattice constant (b) of ϵ -FeOOH is anomalous in Fig. 4(d) further confirms that the length of hydrogen bonds indeed changes in their radial direction. The fact that the O₁ ··· O₂ atom distance decreases with increasing temperature will be discussed in the next section.

It is worth noting that the jumps of the H atoms also occur before reaching the anomalous temperature. This phenomenon is intriguing to contemplate because its occurrence is closely tied to the validity of the calculations in this study. If there is minimal difference in the energy of the H atoms before and after the jump at low temperatures, then the H atoms should not exhibit a preference for the initially closer

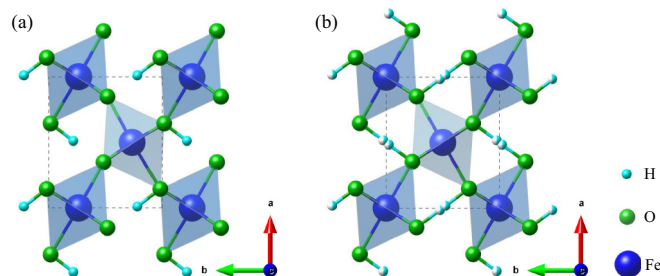


FIG. 6. ϵ -FeOOH at 20 GPa pressure showing (a) $P2_1nm$ structure at 100 K and (b) proton-disordered $Pnmm$ structure at 300 K, with both hydrogen atom positions equally distributed at 50% in $Pnmm$ structure.

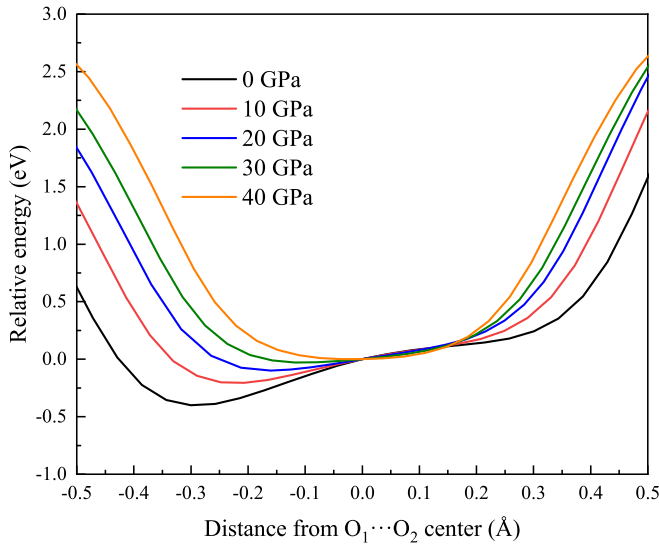


FIG. 7. Variations of system total energy as single H atom moves within $O_1 \cdots H-O_2$ bond at varying pressures, relative to energy when H atom is at hydrogen bond center.

O_1 atoms. In such a scenario, the observed asymmetric distribution of H atoms at low temperatures is likely attributed to slow kinetics and insufficient sampling. To assess the energy difference, we calculated the total system energy for a single H atom moving between two O atoms under static conditions, using the position and system energy when the H atom was at the center of the two O atoms as a reference. We then plotted complete system-energy evolution curves under multiple pressures, as shown in Fig. 7. The left-to-right progression of the curves represents the gradual energy change process as the H atom approaches the O_2 atom, starting from positions near O_1 . Prior to 40 GPa, all curves exhibit a slope at the bottom, with lower energy when the H atom is in proximity to the O_1 atom. At 0 GPa, the lowest energy point of ϵ -FeOOH is located approximately -0.29 \AA from the $O_1 \cdots O_2$ center. We assume that during the disorder-phase transition of ϵ -FeOOH, the H atoms need to jump to the symmetric position at 0.29 \AA . This results in an increase in the system's energy of 0.642 eV . Furthermore, at pressures of 10, 20, and 30 GPa, the energy difference in the system as the H atom moves from its static positions to the symmetric positions is 0.376 , 0.244 , and 0.108 eV , respectively. When the pressure reaches around 40 GPa, ϵ -FeOOH will no longer exhibit significant asymmetric hydrogen bonds, and its energy evolution curve approaches nearly perfect symmetry. These results indicate that the position of H atoms has a stable impact on the total energy of the system, so the asymmetric distribution of H atoms at low temperatures is indeed thermodynamically favorable. Based on these discussions, it can be concluded that the energies required for H atoms to jump are relatively low, suggesting that H atom jumps at low temperatures are a result of localized energy concentration due to temperature fluctuations. However, at this stage, the crystal structure does not possess sufficient symmetry, and H atoms cannot stabilize in their postjump positions, leading them to return to their original positions in a short period. In this scenario, the distribution of H atoms in the two R. positions is unequal. Thus, even if some

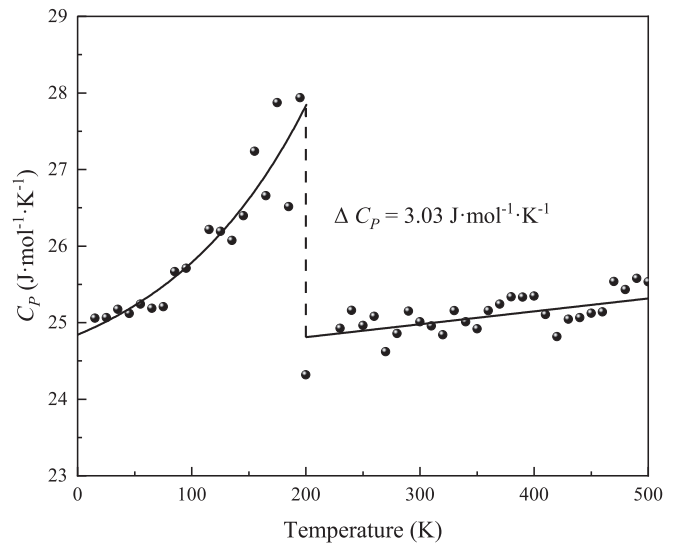


FIG. 8. Molar isobaric heat capacity (C_p) of ϵ -FeOOH during heating process.

H atoms jump, ϵ -FeOOH will maintain the $P2_1nm$ structure. The transition to the higher-symmetry $Pnmm$ structure can only occur when all H atoms are capable of jumping.

The phase transition was reconfirmed from a thermodynamic standpoint, and Fig. 8 displays the molar isobaric heat capacity C_p of ϵ -FeOOH while being heated under 20 GPa pressure. Before reaching 200 K, the C_p of ϵ -FeOOH increases sharply with rising temperature, while C_p decreases abruptly by roughly $3.03 \text{ J mol}^{-1} \text{ K}^{-1}$ after exceeding 200 K. At this temperature, ϵ -FeOOH undergoes a second-order phase transition of proton disordering, as evidenced by the temperature coinciding with the thermal expansion curve anomaly at 20 GPa in Fig. 4(a). More importantly, these findings suggest that the proton-disordering phase transition is the root cause of the anomaly in the system's thermal expansion curve. It is feasible to locate the temperature of the proton-disordering phase transition using this anomaly.

Based on the considerations mentioned above, we might be able to use the anomalies in the thermal expansion curve to identify the conditions for the proton-disordering phase transition of ϵ -FeOOH. However, there exists a challenge here. Due to the short timescales, many dynamics simulations suffer from hysteresis. This means that as the temperature rises, the forces acting on the atoms may not balance promptly, thus preventing the system from reaching a thermal equilibrium state corresponding to the set temperature. Consequently, numerous H atom jumps that were expected at a particular temperature may not have happened, resulting in a delayed appearance of anomalies in the thermal expansion curve, known as the overheating phenomenon. To determine if overheating is present in our study, we employed a method similar to the overheating-undercooling cycle often used in melting studies [53]. If overheating exists, the anomaly point in the cooling process would be lower than that in the heating process. To achieve this, we conducted heating-cooling calculations for ϵ -FeOOH at a pressure of 20 GPa, covering a temperature range of 0–700 K with 10 K intervals. Each 10 K temperature change was simulated for 2 ps, followed

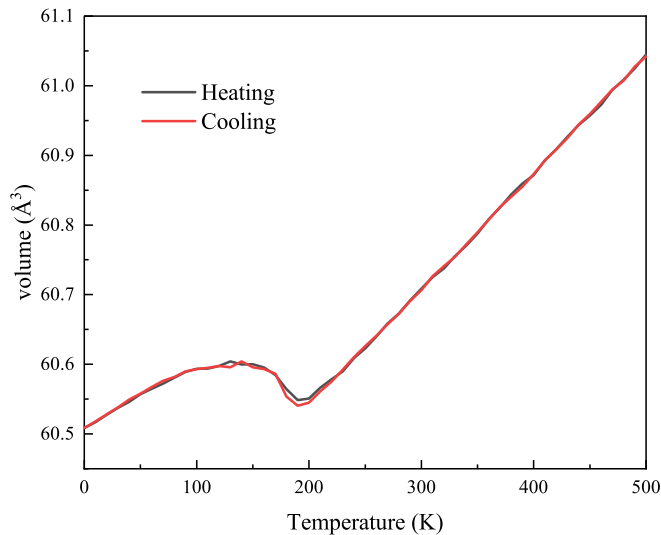


FIG. 9. Volume-temperature curves of ϵ -FeOOH during heating and cooling processes at 20 GPa.

by a 5-ps relaxation after the temperature change. From the results as shown in Fig. 9, it can be found that both the heating and cooling volume-change curves reach their lowest point at 190 K and return to a smooth heating curve at 200 K. The volume-change curves for both the heating and cooling processes are nearly identical. This signifies that there is no overheating phenomenon in the MD process presented in this study. This outcome is foreseeable since the approach used in this study involves a relaxation heating method rather than direct heating, ensuring that the system is close to equilibrium at each temperature point. Moreover, the proton-disordering phase transition, as a second-order transition, does not require a substantial accumulation of energy to overcome the phase-transition barrier. These aspects ensure that employing the anomalous points in the thermal expansion curve to judge the proton-disordering phase transition from $P2_1nm$ to Pnm structure in ϵ -FeOOH is a sufficiently reliable method.

Importantly, we emphasize that the DP model exhibits remarkable accuracy when compared to the empirical potential function. However, due to the intrinsic nature of the machine learning approach, our potential function faces the challenge of providing highly accurate results for states that deviate significantly from the fitted condition. Fortunately, the temperature and pressure conditions investigated in this study remain within moderate ranges, thereby circumventing this problem. Furthermore, we also need to elucidate that in various hydrogen-bonded compounds such as δ -AlOOH and ice, there exists the quantum effect of proton tunneling [54–57]. However, the DP model still adheres to Newton’s laws of motion. Therefore, we are unable to discuss the potential proton tunneling effects present in ϵ -FeOOH within the scope of this methodology employed in our study. These limitations are inherent to the approach used in this study.

III. RESULTS AND DISCUSSION

A. Hydrogen bond symmetrization at 0 K

The hydrogen bond symmetrization pressure of ϵ -FeOOH is difficult to determine in part because the H atom is a weak

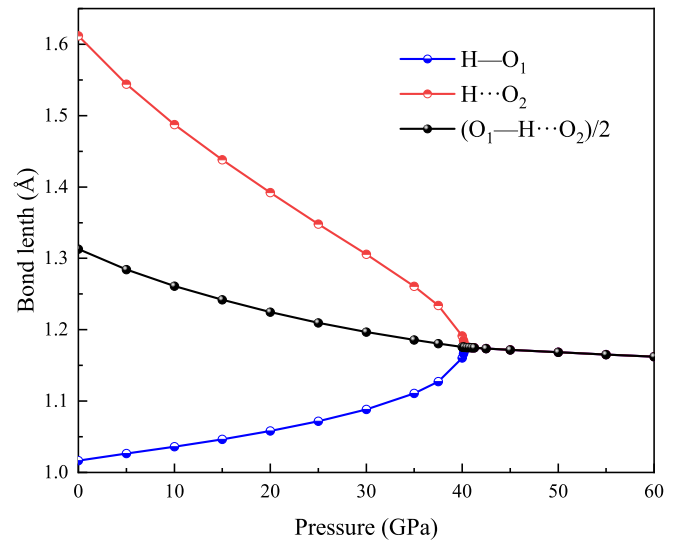


FIG. 10. Correlation between O—H bond length and pressure for ϵ -FeOOH.

x-ray scatterer, which is usually undetectable in experiments, so it is experimentally difficult to determine this phase-transition pressure by measuring bond lengths, but hydrogen bond symmetrization or disorder induces subtle changes in lattice strain, as some previous studies on AlOOH used indirect measurements to obtain hydrogen bond symmetrization pressure [15,17,58]. Tompson *et al.* [21] recently determined a hydrogen bond symmetrization or disorder pressure of about 18 GPa for ϵ -FeOOH by judging the abrupt change in the lattice constant ratio with increasing pressure. Xu *et al.* [20] determined this phase-transition pressure by tracing the sudden decrease in the twisted structure of the FeO_6 octahedra forming the crystal structure and finally obtained that the hydrogen bond symmetrization pressure may exceed 44 GPa.

Fortunately, computer simulation methods allow easy O—H bond length access. We performed static calculations of the ϵ -FeOOH hydrogen bond symmetrization pressure using the DP model, and the results are shown in Fig. 10. The H—O₁ bond length at zero pressure is 1.02 Å, the H···O₂ bond is 1.61 Å, and the O₁···O₂ spacing is 2.63 Å, which is in full agreement with the calculations of Gleason *et al.* [11] and close to the experimental result of Bolotina *et al.* of 2.67 Å [16], and the bond lengths of the O₁—H···O₂ bonds during the pressure increase show a uniformly decreasing trend and hydrogen bond symmetrization occurs when the pressure reaches 40.25 GPa, at which time the O—H bond lengths are both 1.175 Å. This is expressed macroscopically as a continuous change in the volume of ϵ -FeOOH during the compression process.

B. Proton-disordering phase transition

At zero temperature, we can only observe a transition of hydrogen bonding from asymmetric to symmetric, without obtaining any information about the proton-disordering phase transition. As a precursor structure to symmetric hydrogen bonding, we must precisely determine the conditions for the proton-disordering phase transition. We have already

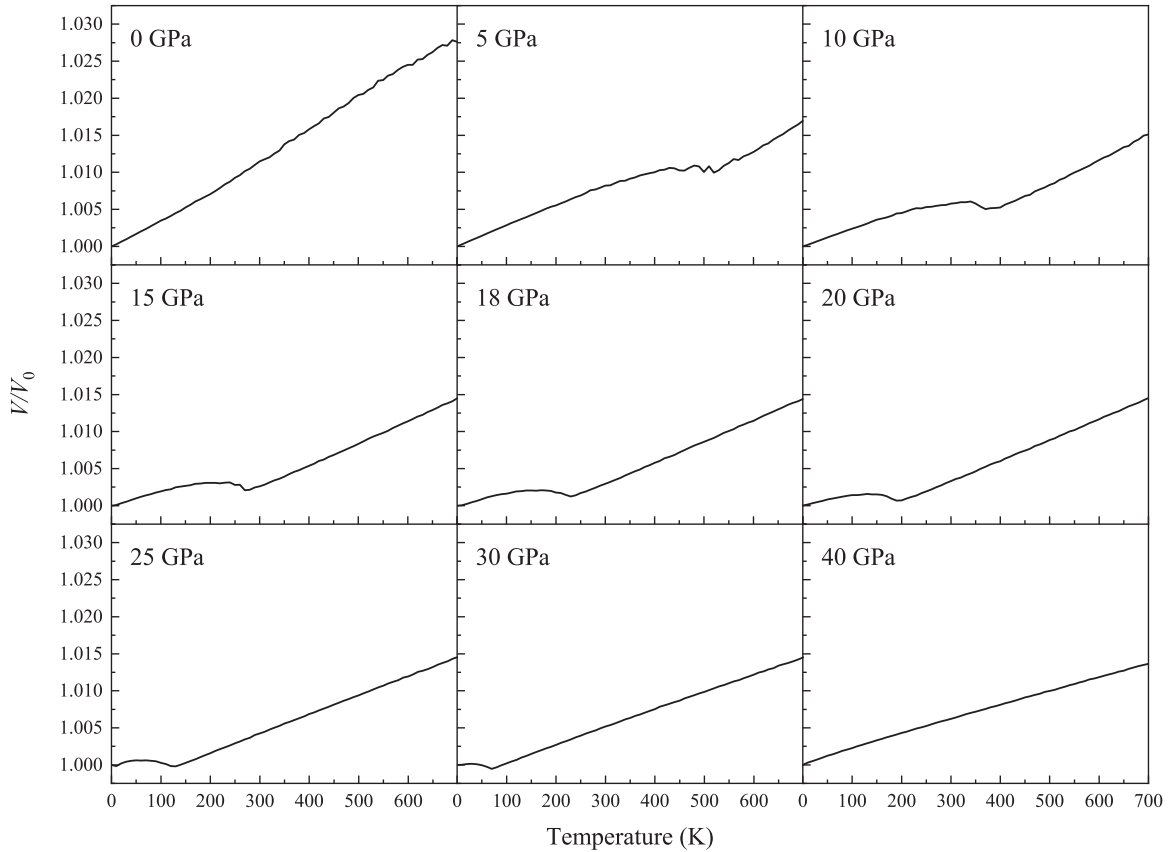


FIG. 11. ϵ -FeOOH in pressure range of 0–40 GPa for volume ratio–temperature curves.

demonstrated that an increase in temperature leads to proton disorder, specifically the transition from the $P2_1nm$ to $Pnmm$ structure, resulting in anomalous behavior in the volume expansion curve. This allows us to definitively identify the phase-transition boundary of proton disorder. We heated ϵ -FeOOH from 0 to 700 K at 10 K intervals under several pressure conditions to find anomalies in the volume thermal expansion curve of ϵ -FeOOH during the heating process, and the calculated results are shown in Fig. 11. The volume thermal expansion curves at both 0 and 40-GPa pressures show a smooth increase with temperature, which indicates that ϵ -FeOOH is a pure phase at both pressures. We considered that ϵ -FeOOH does not have an energy advantage at 0 GPa pressure, so it was not taken into account in the subsequent work. The pressure of 40 GPa is very close to the hydrogen bond symmetrization pressure of 40.25 GPa. Therefore, at 40 GPa, the hydrogen atoms are already at a critical position, requiring only a slight increase in temperature to induce a phase transition in ϵ -FeOOH, thus exhibiting individual phase characteristics. The volume thermal expansion curves of ϵ -FeOOH showed anomalous troughs at several pressures ranging from 5 to 30 GPa. The lines connecting these temperature and pressure points corresponding to the volume minima constitute the phase-transition boundary from $P2_1nm$ to $Pnmm$ structures. We have depicted these data along with the ultimately determined boundary for hydrogen bond symmetrization (see Fig. 16).

The pressure of proton disorder in ϵ -FeOOH is strongly influenced by temperature (see Fig. 16). The phase-transition

pressure at 300 K is determined to be 14.4 GPa, which is close to the value of 18 GPa obtained by Thompson *et al.* [21] through x-ray-diffraction experiments at 300 K. At 0 K, the proton-disordered structure does not exist, and only the hydrogen bond symmetrization phase transition occurs. Our determined phase-transition pressure for this scenario is 40.25 GPa, which is also in close agreement with the first-principles calculation result of 43 GPa obtained by Gleason *et al.* [11]. Hence, the significant discrepancies in hydrogen bond symmetrization pressures may be attributed to the proton-disorder configurations detected by Thompson *et al.* [21], along with the pronounced temperature-dependent behavior of the proton-disordering phase-transition pressure. This conclusion is expected to be applied to the same type of $AlOOH(D)$, $CrOOH(D)$, $GaOOH$, $InOOH$, and other similar minerals.

To comprehend the fundamental reasons behind the variation in proton-disordering phase-transition pressure with temperature, we need to consider it from the perspective of hydrogen bonding. In hydrated minerals like ϵ -FeOOH, hydrogen bonds exhibit dual potential wells [19]. As the temperature rises, the energy of the hydrogen atom progressively increases, causing its vibrational range to span both potential wells between two O atoms. The energy associated with hopping can surpass the energy barrier, allowing the hydrogen atom to leap from its original position to another equilibrium position. However, at lower temperatures and pressures, the hydrogen atoms cannot remain stable in the shallower potential well because of the different depths of the two potential

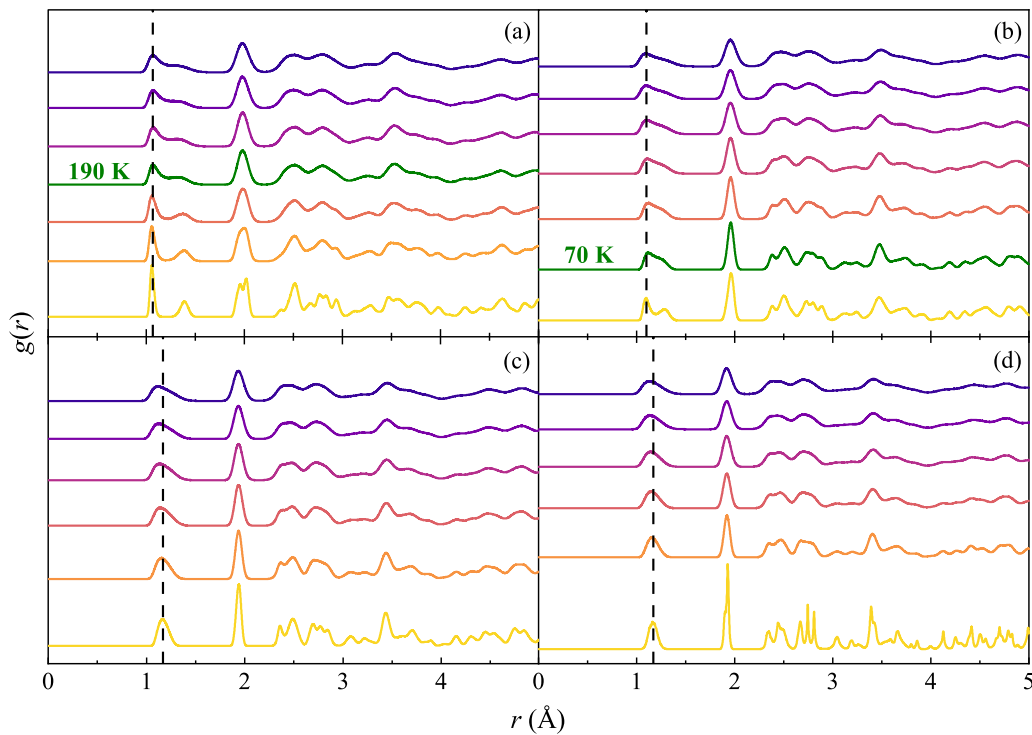


FIG. 12. Radial distribution functions $g(r)$ of ϵ -FeOOH at (a) 20 GPa, (b) 30 GPa, (c) 40 GPa, and (d) 50 GPa, from yellow to dark blue lines, indicate $g(r)$ at 50–300 K with interval of 50 K, respectively, and green lines indicate $g(r)$ reaching phase-transition temperature.

wells, causing them to frequently return to their initial positions. Consequently, the probability of the hydrogen atom appearing on the two potential wells is unequal, rendering it premature to term this state as proton disorder. At higher temperatures, the hydrogen atom vibrates vigorously, even in the deeper potential well. This kinetic energy far exceeds the energy barrier on one side of the deeper well, significantly enhancing the probability of the hydrogen atom being captured by the shallow potential well. When each vibration of the hydrogen atom can span the distance between the dual potential wells and be captured by either well, the probability of its occurrence on the two wells becomes equal. This marks a true proton-disordered structure. The temperature of the proton-disordering phase transition decreases with increasing pressure. The fundamental reason behind this lies in the fact that elevated pressure causes the dual potential wells in hydrogen bonds to approach each other, leading to a decrease in the energy barrier between them, which we can find in the energy curve shown in Fig. 7. Consequently, the energy required for the hydrogen atom to surpass the barrier restriction and leap decreases in tandem, resulting in a synchronous decrease in temperature. The dual potential wells in the hydrogen bond merge at pressures up to 40.25 GPa, and the temperature of the disordered phase transition drops to 0 K.

C. Critical conditions for hydrogen bond symmetrization

We can determine that the dual potential wells are separated before reaching 40.25 GPa. At this point, raising the temperature will invariably result in proton disorder. However, beyond a pressure of 40.25 GPa, whether hydrogen bonds indeed undergo symmetrization becomes uncertain. Therefore,

the next step is to distinguish between proton disorder and hydrogen bond symmetrization structures. Yet, discerning these two structures poses a challenge. Experimentally, the diffraction patterns produced by these two structures are nearly indistinguishable [21,22], and this computational study encounters similar difficulties. We initially attempted to compute the radial distribution function $g(r)$ (RDF) [59] of ϵ -FeOOH to differentiate its crystal structures under different conditions. RDF can be interpreted as the density of other particles at a distance r from a reference particle and is a common method for judging crystal structures. Given that the hopping or symmetrization behavior of protons within the crystal might have a certain probability, the $g(r)$ function was time averaged to obtain more accurate statistical results.

As shown in Fig. 12, we present the $g(r)$ for ϵ -FeOOH during the heating process under pressures ranging from 20 to 50 GPa. The first two peak positions of the $g(r)$ curve correspond to the bond lengths of H—O₁ and H···O₂. It can be observed that at 20 GPa, as the temperature increases, the $g(r)$ curve of ϵ -FeOOH tends to merge the two peaks. Beyond the phase-transition temperature of 190 K, the valley between the two peaks disappears, gradually forming a plateau. As the temperature continues to rise, the second peak gradually merges with the original peak, forming a nearly smooth curve. The reason for the plateau is that the density of hydrogen atoms in the two equilibrium positions is higher than that in the middle, indicating that the movement path of hydrogen atoms is not continuous. When the temperature is sufficiently high, the frequency of hydrogen atoms appearing in the middle position also becomes quite high, resulting in a slightly more uniform density along the entire movement path and leading to the smoothing of the $g(r)$ peaks. At a pressure of

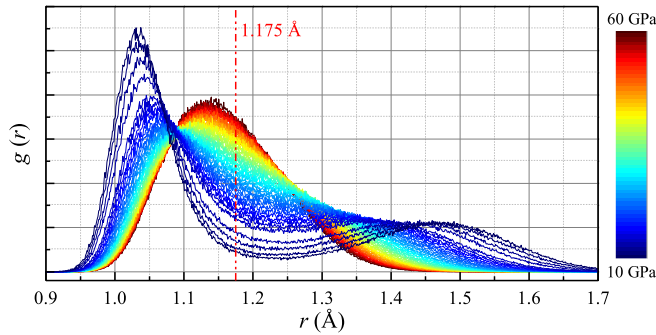


FIG. 13. Variation of $g(r)$ with pressure for ϵ -FeOOH at 300 K.

30 GPa, after reaching a temperature of 70 K, the valley between the two peaks of ϵ -FeOOH's $g(r)$ suddenly disappears, and the characteristics of the second peak gradually diminish with increasing temperature. Under pressures of 40 and 50 GPa, the $g(r)$ at all temperatures shows only one H-O peak and becomes quite smooth. However, while the structure at 40 GPa should correspond to proton disorder, and the structure at 50 GPa should be hydrogen bond symmetrization, there is no discernible difference between them in the $g(r)$. To delve deeper into the pressure dependence of $g(r)$, we once again computed the $g(r)$ of ϵ -FeOOH at a fixed temperature of 300 K under varying pressures. The exploration range was expanded to 10–60 GPa, and the pressure increments were reduced to 1 GPa. The results are shown in Fig. 13. In the process of increasing the pressure, $g(r)$ evolves rapidly from the initial case with two distinct peaks to a single peak. At about 30-GPa pressure (cyan region) the rate of change of $g(r)$ slows down and the position of its peak begins to show a slight rightward shift. The $g(r)$ of ϵ -FeOOH is already difficult to distinguish from the diagram after the pressure exceeds 30 GPa, which also indicates that the proton-disordered structure and the hydrogen bond symmetry structure of ϵ -FeOOH are almost the same at this time. Essentially, this is because the H atoms in both the proton-disordered and hydrogen bond symmetrization structures vibrate on the centerline of two O atoms, and the H—O₁ and H⋯O₂ bond lengths are extremely close to each other, which leads to the fact that the vibrational behavior of the H atoms in both structures tends to be the same, and the two structures can no longer be considered significantly different at high temperature and pressure conditions. This situation implies that even the approach of judging by H—O bond lengths cannot precisely determine the pressure of hydrogen bond symmetrization.

Additionally, these $g(r)$ curves exhibit some perplexing phenomena. In Fig. 12, for pressures exceeding 30 GPa, the first peak of $g(r)$ shifts to the left with increasing temperature, suggesting that the H—O bond becomes shorter as the temperature rises. And, in Fig. 13, although the peak value of the first peak of $g(r)$ increases with pressure, even at 60 GPa, its peak position is still far from the bond length of 1.175 Å, which corresponds to the hydrogen bond symmetrization occurring at zero temperature. This indicates that the increase in temperature does indeed lead to a reduction in the H—O bond length. However, at 60 GPa, the hydrogen bonds should already be symmetric. We first ruled out the possibility

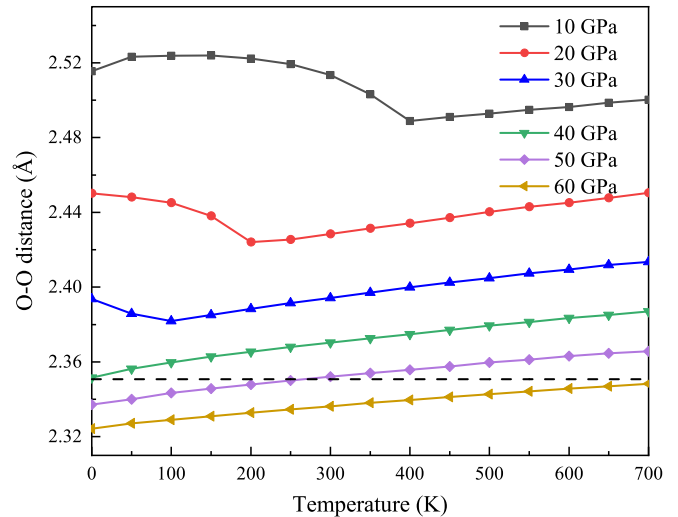


FIG. 14. Variation of O₁⋯O₂ atomic distance in ϵ -FeOOH at different pressures with temperature; black dashed line represents critical hydrogen bond symmetrization O₁⋯O₂ atomic distance 2.351 Å.

of the H—O bond length corresponding to hydrogen bond symmetrization decreasing with temperature. After hydrogen bond symmetrization, the H—O₁ and H⋯O₂ bond lengths are equal. If the H—O bond length were to decrease with increasing temperature after hydrogen bond symmetrization, then the O₁⋯O₂ distance would also change synchronously. We computed the O₁⋯O₂ atomic distances at different pressures, as shown in Fig. 14. Under pressures of 10 to 30 GPa, at lower temperatures, the O₁⋯O₂ atomic distance decreases with increasing temperature, while at higher temperatures, it increases with temperature. The inflection point of the O₁⋯O₂ atomic distance change corresponds precisely to the proton-disordering phase-transition temperature determined in this study. This once again underscores the connection between the anomaly in the volume thermal expansion curve and the proton-disordering phase-transition behavior. Under pressures of 40 to 60 GPa, the O₁⋯O₂ atomic distance of ϵ -FeOOH remains positively correlated with temperature. This implies that the reason for the leftward shift of the first peak in the $g(r)$ curve is not a decrease in the hydrogen bond symmetrization bond length due to temperature, but rather an increase in temperature causing the O₁⋯O₂ atomic distance to enlarge. This reopens the dual potential well for the hydrogen atom, leading to the phenomenon of the H—O₁ bond length appearing to shorten due to the increased O₁⋯O₂ atomic distance, as illustrated in Fig. 10. This also confirms the close relationship between H—O bond lengths and O₁⋯O₂ atomic distances. In fact, Meier *et al.* [23] have already discovered that hydrogen bond symmetrization occurs within the narrow range of O₁⋯O₂ distances between 2.44–2.45 Å, independently of the surrounding chemical environment, which means that the O₁⋯O₂ atomic distance in hydrogen bond symmetrization is fixed. So, the observed phenomenon of shortened H—O bond lengths in the $g(r)$ curve is a result of the increase in temperature leading to the degradation of the symmetric hydrogen bond structure

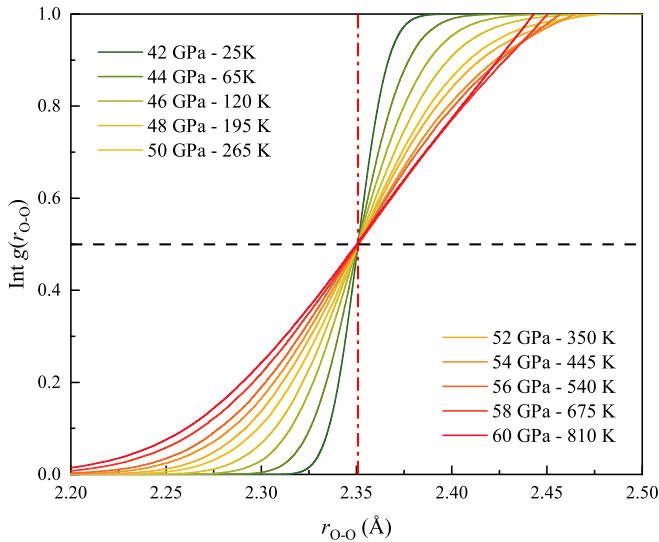


FIG. 15. Int $g(r_{O-O})$ of proton-disorder–hydrogen bond symmetrization equilibrium point in ϵ -FeOOH.

into a proton-disordered structure. Therefore, we can initially conclude that the pressure of hydrogen bond symmetrization will increase with rising temperature, and the specific pressure value can be accurately determined by calculating the critical $O_1 \cdots O_2$ atomic distance for hydrogen bond symmetrization at high temperatures.

The $O_1 \cdots O_2$ atomic distance at 40.25 GPa pressure is 2.351 Å, denoted as d_{O-O}^H , represented by the black dashed line in Fig. 14. This value reflects atomic interactions in the MD simulation method and remains unaffected by changes in temperature or pressure. Therefore, it can serve as a criterion for determining hydrogen bond symmetrization. At 40 GPa pressure, the $O_1 \cdots O_2$ atomic distance in the 0 K is slightly larger than d_{O-O}^H , and as temperature rises, the $O_1 \cdots O_2$ distance gradually deviates from d_{O-O}^H . For the $O_1 \cdots O_2$ atomic distance curve at 50 GPa, it intersects with d_{O-O}^H around 265 K. And, for the 60-GPa pressure case, the $O_1 \cdots O_2$ atomic distance curve remains consistently below d_{O-O}^H within the 0–700 K range.

To pinpoint the boundary between proton-disordered and hydrogen bond symmetrization structures, we calculated the average $O_1 \cdots O_2$ atomic distance of ϵ -FeOOH at intervals of 2 GPa, with a temperature increment of 5 K. Eventually, we determined temperature-pressure points within the 40.25–60-GPa pressure range where the $O_1 \cdots O_2$ atomic distance coincides with 2.351 Å. During this process, we noticed that at elevated temperatures, oxygen atoms exhibit vibrations over a broader range, causing the $O_1 \cdots O_2$ atomic distance to frequently exceed d_{O-O}^H , leading to the reappearance of hydrogen atom double-potential wells. Conversely, these distances sometimes become shorter than d_{O-O}^H , causing the dual potential wells to merge. This suggests that the identified temperature-pressure conditions are equilibrium points between proton-disordered and hydrogen bond symmetrization structures. At all established temperature-pressure points, the integral of the radial distribution function Int $g(r_{O-O})$ remains consistently at 0.5 below d_{O-O}^H (Fig. 15). This implies that only 0.5 of an atom exists below the equilibrium position of O

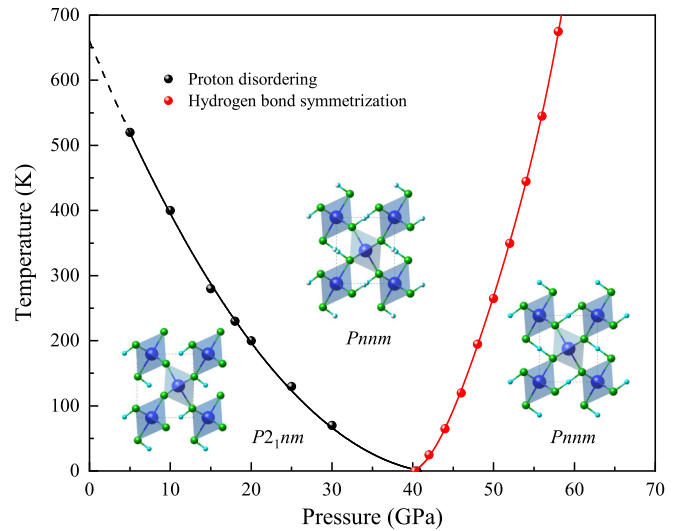


FIG. 16. Phase diagram of ϵ -FeOOH, where black and red lines represent fitted boundaries for proton-disordering phase transition and the critical hydrogen bond symmetrization, respectively.

atoms, and the number of nearest-neighboring O atoms for an O atom is 1, corresponding to half of the $O_1 \cdots O_2$ atomic distances being smaller than 2.351 Å. Consequently, we can infer that after surpassing these temperature and pressure points, the hydrogen bond symmetrization structure gains more dominance. While localized proton disordering still exists within the crystal, the presence of these disordered protons leads to the phenomenon of the first peak in the $g(r)$ curve, representing the H-O atomic distance, shortening with increasing temperature. These discussions also indicate that hydrogen bond symmetrization is a continuous process. Defining the phase-transition point for hydrogen bond symmetrization at high temperatures might not be entirely precise; hence, we refer to it as the critical point.

D. Phase diagram

Finally, we have combined the critical points identified for proton disordering and hydrogen bond symmetrization, along with the previously computed points for proton-disordering phase transition, to construct a comprehensive hydrogen bond symmetrization phase diagram for ϵ -FeOOH. Figure 16 illustrates that the critical pressure for proton-disordering phase transition decreases with increasing temperature, while the critical pressure for hydrogen bond symmetrization increases with temperature. These two boundaries intersect at the temperature and pressure conditions of 0 K and 40.25 GPa, respectively. As the system temperature rises, the range of pressures in which the proton-disordering phase transition occurs expands. Even beyond the boundary of the hydrogen bond symmetrization structure, localized proton-disordered structures continue to persist. Importantly, existing research indicates that ϵ -FeOOH undergoes a spin transition within the pressure range of 40–60 GPa [11,20], leading to a volume reduction of approximately 11%, and this reduction causes a decrease in the $O_1 \cdots O_2$ atomic distance. Considering that the occurrence of hydrogen bond symmetrization is independent of the chemical environment and solely determined by the

$O_1 \cdots O_2$ atomic distance, the spin transition of Fe induces a transition of ε -FeOOH from proton-disordered to hydrogen bond symmetrization structure. However, at lower temperatures, the influence of pressure on the $O_1 \cdots O_2$ atomic distance is already sufficient to trigger hydrogen bond symmetrization. At this point, the spin transition of Fe becomes unrelated to hydrogen bond symmetrization. In other words, the correlation between hydrogen bond symmetrization and the spin transition of Fe is greatly influenced by temperature. In summary, there is no inherent connection between the two phenomena; they are separate and independent processes. This might also explain the underlying reason for the discrepancies observed in the relationship between Fe atoms' spin transition and hydrogen bond symmetrization.

IV. CONCLUSION

In summary, the hydrogen bond symmetrization of ε -FeOOH is a continuous phase-transition process, proton disorder is the precursor of hydrogen bond symmetrization, and the phase-transition pressure from hydrogen bond asymmetry to proton disorder ($P2_1nm \rightarrow Pnm$) has a strong temperature dependence which leads to a large discrepancy between indirect experimental results and static computer simulations. The critical temperature for hydrogen bond symmetrization will increase with the rise in pressure, primarily due to the enlargement of $O_1 \cdots O_2$ atomic distances. However, when both high temperature and high pressure are considered, the

large amplitude of the H atoms leads to the fact that there is no longer a clear distinction between the hydrogen-bonded symmetrization structure and the proton-disorder structure, which is why the experimental diffraction patterns of the two are almost identical [21,22]. Furthermore, the correlation between hydrogen bond symmetrization and the spin transition of Fe is greatly influenced by temperature. Hydrogen bond symmetrization still takes place in ε -FeOOH even when the spin transition of Fe atoms is not considered at lower temperatures. However, as the temperature increases, the critical pressure for hydrogen bond symmetrization will also rise with temperature. When spin transitions occur, hydrogen bond symmetrization may be promoted. Our computational findings offer insights for investigating the symmetrization process of hydrogen bonds within compounds of the same category. More specifically, by measuring the variations in material volume and $O_1 \cdots O_2$ atomic distance with temperature, one will have the opportunity to explore the complete transition process of hydrogen bonds from asymmetric to symmetric structures. This experimental approach holds promise as a viable solution until direct probing of hydrogen atoms becomes feasible.

ACKNOWLEDGMENT

Support from the National Natural Science Foundation of China (Grants No. 51562021 and No. 11464027) is gratefully acknowledged.

-
- [1] E. Koemets, T. Fedotenko, S. Khandarkhaeva, M. Bykov, E. Bykova, M. Thielmann, S. Chariton, G. Aprilis, I. Koemets, and K. Glazyrin, *Eur. J. Inorg. Chem.* **2021**, 3048 (2021).
 - [2] J. Liu, Q. Hu, D. Young Kim, Z. Wu, W. Wang, Y. Xiao, P. Chow, Y. Meng, V. B. Prakapenka, and H.-K. Mao, *Nature (London)* **551**, 494 (2017).
 - [3] H.-K. Mao, Q. Hu, L. Yang, J. Liu, D. Y. Kim, Y. Meng, L. Zhang, V. B. Prakapenka, W. Yang, and W. L. Mao, *Natl. Sci. Rev.* **4**, 870 (2017).
 - [4] T. Nagai, H. Kagi, and T. Yamanaka, *Am. Mineral.* **88**, 1423 (2003).
 - [5] A. Szytuła, A. Burewicz, Ž. Dimitrijević, S. Krašnicki, H. Ržany, J. Todorović, A. Wanic, and W. Wolski, *Phys. Status Solidi B* **26**, 429 (1968).
 - [6] A. Mackay, *Miner. Mag.* **32**, 545 (1960).
 - [7] K. Otte, R. Pentcheva, W. W. Schmahl, and J. R. Rustad, *Phys. Rev. B* **80**, 205116 (2009).
 - [8] M. Pernet, J. C. Joubert, and C. Berthet-Colominas, *Solid State Commun.* **17**, 1505 (1975).
 - [9] C. Lu and C. Chen, *J. Phys. Chem. Lett.* **9**, 2181 (2018).
 - [10] E. C. Thompson, A. Campbell, and J. Tsuchiya, *J. Geophys. Res.: Solid Earth* **122**, 5038 (2017).
 - [11] A. E. Gleason, C. E. Quiroga, A. Suzuki, R. Pentcheva, and W. L. Mao, *Earth Planet. Sci. Lett.* **379**, 49 (2013).
 - [12] M. M. Reagan, A. E. Gleason, L. Daemen, Y. Xiao, and W. L. Mao, *Am. Mineral.* **101**, 1483 (2016).
 - [13] Q. Hu, D. Y. Kim, W. Yang, L. Yang, Y. Meng, L. Zhang, and H.-K. Mao, *Nature (London)* **534**, 241 (2016).
 - [14] M. Nishi, Y. Kuwayama, J. Tsuchiya, and T. Tsuchiya, *Nature (London)* **547**, 205 (2017).
 - [15] A. Sano-Furukawa, H. Kagi, T. Nagai, S. Nakano, S. Fukura, D. Ushijima, R. Iizuka, E. Ohtani, and T. Yagi, *Am. Mineral.* **94**, 1255 (2009).
 - [16] N. B. Bolotina, V. N. Molchanov, T. I. Dyuzheva, L. M. Lityagina, and N. A. Bendeliani, *Crystallogr. Rep.* **53**, 960 (2008).
 - [17] A. Sano-Furukawa, T. Yagi, T. Okada, H. Gotou, and T. Kikegawa, *Phys. Chem. Miner.* **39**, 375 (2012).
 - [18] K. Aoki, H. Yamawaki, M. Sakashita, and H. Fujihisa, *Phys. Rev. B* **54**, 15673 (1996).
 - [19] J. Tsuchiya and E. C. Thompson, *Prog. Earth Planet. Sci.* **9**, 63 (2022).
 - [20] W. Xu, E. Greenberg, G. K. Rozenberg, M. P. Pasternak, E. Bykova, T. Boffa-Ballaran, L. Dubrovinsky, V. Prakapenka, M. Hanfland, O. Y. Vekilova, S. I. Simak, and I. A. Abrikosov, *Phys. Rev. Lett.* **111**, 175501 (2013).
 - [21] E. C. Thompson, A. H. Davis, N. M. Brauser, Z. Liu, V. B. Prakapenka, and A. J. Campbell, *Am. Mineral.* **105**, 1769 (2020).
 - [22] T. Fujihara, M. Ichikawa, T. Gustafsson, I. Olovsson, and T. Tsuchida, *J. Phys. Chem. Solids* **63**, 309 (2002).
 - [23] T. Meier, F. Trybel, S. Khandarkhaeva, D. Laniel, T. Ishii, A. Aslandukova, N. Dubrovinskaja, and L. Dubrovinsky, *Nat. Commun.* **13**, 3042 (2022).
 - [24] M. Aryanpour, A. C. van Duin, and J. D. Kubicki, *J. Phys. Chem. A* **114**, 6298 (2010).

- [25] L. Zhang, J. Han, H. Wang, R. Car, and Weinan E, *Phys. Rev. Lett.* **120**, 143001 (2018).
- [26] J. Han, L. Zhang, R. Car, and Weinan E, *Commun. Comput. Phys.* **23**, 629 (2018).
- [27] J. Behler and M. Parrinello, *Phys. Rev. Lett.* **98**, 146401 (2007).
- [28] S. Chmiela, A. Tkatchenko, H. E. Sauceda, I. Poltavsky, K. T. Schütt, and K.-R. Müller, *Sci. Adv.* **3**, e1603015 (2017).
- [29] A. P. Bartók, M. C. Payne, R. Kondor, and G. Csányi, *Phys. Rev. Lett.* **104**, 136403 (2010).
- [30] A. P. Thompson, L. P. Swiler, C. R. Trott, S. M. Foiles, and G. J. Tucker, *J. Comput. Phys.* **285**, 316 (2015).
- [31] A. Sano-Furukawa, T. Hattori, K. Komatsu, H. Kagi, T. Nagai, J. J. Molaison, A. M. Dos Santos, and C. A. Tulk, *Sci. Rep.* **8**, 15520 (2018).
- [32] S. Plimpton, *J. Comput. Phys.* **117**, 1 (1995).
- [33] G. Kresse and J. Hafner, *Phys. Rev. B* **47**, 558 (1993).
- [34] G. Kresse and J. Furthmüller, *Phys. Rev. B* **54**, 11169 (1996).
- [35] G. Kresse and J. Furthmüller, *Comput. Mater. Sci.* **6**, 15 (1996).
- [36] J. P. Perdew, K. Burke, and M. Ernzerhof, *Phys. Rev. Lett.* **77**, 3865 (1996).
- [37] V. I. Anisimov, I. V. Solovyev, M. A. Korotin, M. T. Czyżyk, and G. A. Sawatzky, *Phys. Rev. B* **48**, 16929 (1993).
- [38] I. Leonov, A. N. Yaresko, V. N. Antonov, M. A. Korotin, and V. I. Anisimov, *Phys. Rev. Lett.* **93**, 146404 (2004).
- [39] G. Rollmann, A. Rohrbach, P. Entel, and J. Hafner, *Phys. Rev. B* **69**, 165107 (2004).
- [40] T. Tsuchiya, R. M. Wentzcovitch, C. R. S. da Silva, and S. de Gironcoli, *Phys. Rev. Lett.* **96**, 198501 (2006).
- [41] See Supplemental Material at <http://link.aps.org/supplemental/10.1103/PhysRevB.108.184105> for validation of the Hubbard parameters, testing of the accuracy of the AIMD calculations, and the probability distribution functions for O and Fe atoms.
- [42] I. V. Solovyev, P. H. Dederichs, and V. I. Anisimov, *Phys. Rev. B* **50**, 16861 (1994).
- [43] P. E. Blöchl, *Phys. Rev. B* **50**, 17953 (1994).
- [44] H. J. Monkhorst and J. D. Pack, *Phys. Rev. B* **13**, 5188 (1976).
- [45] S. Nosé, *J. Chem. Phys.* **81**, 511 (1984).
- [46] W. G. Hoover, *Phys. Rev. A* **31**, 1695 (1985).
- [47] H. Wang, L. Zhang, J. Han, and E. Weinan, *Comput. Phys. Commun.* **228**, 178 (2018).
- [48] L. Zhang, J. Q. Han, H. Wang, W. Saidi, R. Car, and Weinan E, *Adv. Neural Inf. Process. Syst.* **31**, 4436 (2018).
- [49] A. E. Gleason, R. Jeanloz, and M. Kunz, *Am. Mineral.* **93**, 1882 (2008).
- [50] O. Ikeda, T. Sakamaki, T. Ohashi, M. Goto, Y. Higo, and A. Suzuki, *J. Miner. Petrol. Sci.* **114**, 155 (2019).
- [51] A. Suzuki, *Phys. Chem. Miner.* **37**, 153 (2010).
- [52] T. Sun, D.-B. Zhang, and R. M. Wentzcovitch, *Phys. Rev. B* **89**, 094109 (2014).
- [53] Y. Zou, S. Xiang, and C. Dai, *Comput. Mater. Sci.* **171**, 109156 (2020).
- [54] F. Trybel, T. Meier, B. Wang, and G. Steinle-Neumann, *Phys. Rev. B* **104**, 104311 (2021).
- [55] L. Lin, J. A. Morrone, and R. Car, *J. Stat. Phys.* **145**, 365 (2011).
- [56] T. Meier, S. Petitgirard, S. Khandarkhaeva, and L. Dubrovinsky, *Nat. Commun.* **9**, 2766 (2018).
- [57] F. Trybel, M. Cosacchi, T. Meier, V. M. Axt, and G. Steinle-Neumann, *Phys. Rev. B* **102**, 184310 (2020).
- [58] T. Kuribayashi, A. Sano-Furukawa, and T. Nagase, *Phys. Chem. Miner.* **41**, 303 (2014).
- [59] B. G. Levine, J. E. Stone, and A. Kohlmeyer, *J. Comput. Phys.* **230**, 3556 (2011).